



MIT Open Access Articles

Efficient Perovskite Solar Cells Based on CdSe/ZnS Quantum Dots Electron Transporting Layer with Superior UV Stability

The MIT Faculty has made this article openly available. **Please share** how this access benefits you. Your story matters.

Citation	Tavakoli, Mohammad Mahdi, Prochowicz, Daniel, Yadav, Pankaj and Tavakoli, Rouhollah. 2020. "Efficient Perovskite Solar Cells Based on CdSe/ZnS Quantum Dots Electron Transporting Layer with Superior UV Stability." physica status solidi (RRL) – Rapid Research Letters, 14 (6).
As Published	http://dx.doi.org/10.1002/pssr.202000062
Publisher	Wiley
Version	Author's final manuscript
Citable link	https://hdl.handle.net/1721.1/140935
Terms of Use	Article is made available in accordance with the publisher's policy and may be subject to US copyright law. Please refer to the publisher's site for terms of use.

Efficient Perovskite Solar Cells Based on CdSe/ZnS Quantum Dots Electron Transporting Layer with Superior UV Stability

Mohammad Mahdi Tavakoli,^{1,2}*Daniel Prochowicz,³ Pankaj Yadav,⁴ Rouhollah Tavakoli²

¹Department of Electrical Engineering and Computer Science, Massachusetts Institute of Technology, Cambridge, MA 02139, USA

²Department of Materials Science and Engineering, Sharif University of Technology, 14588 Tehran, Iran

³Institute of Physical Chemistry, Polish Academy of Sciences, Kasprzaka 44/52, 01-224 Warsaw, Poland

⁴Department of Solar Energy, School of Technology, Pandit Deendayal Petroleum University, Gandhinagar-382 007, Gujarat, India

* Corresponding author: mtavakol@mit.edu (M. M. T.)

Abstract

Stability is the main challenge in the field of perovskite solar cells (PSCs). Finding new strategies is required to protect the PSCs from deteriorated agents such as humidity, heating, and illumination. In this study, we propose a new electron transporting layer (ETL), i.e., CdSe/ZnS quantum dots (QDs) for the fabrication of efficient and stable PSCs. CdSe/ZnS QDs layer not only works as an ETL but also has down-shifting property, which can improve both efficiency and stability of the PSCs. Using CdSe/ZnS QDs ETL with green emission, a PSC with maximum power conversion efficiency (PCE) of 18% is achieved. More importantly, our device shows great UV stability much better than the device with TiO₂ ETL, where it retains 90% of its initial PCE value after 75 h under continuous UV illumination.

This is the author manuscript accepted for publication and has undergone full peer review but has not been through the copyediting, typesetting, pagination and proofreading process, which may lead to differences between this version and the [Version of Record](#). Please cite this article as [doi: 10.1002/pssr.202000062](https://doi.org/10.1002/pssr.202000062).

This article is protected by copyright. All rights reserved

Keywords: CdSe/ZnS QDs, perovskite, solar cell, stability, UV stability, down-shifting layer

Introduction

Organic-inorganic perovskite materials with their outstanding optoelectronic properties have made a revolution in the field of optoelectronic devices.¹⁻⁸ Among all thin film photovoltaics (PVs), perovskite solar cells (PSCs) show a fast progress in a short period of time with high efficiency exceeding 25%, thanks to their great absorption, long diffusion length, high quality crystals, low-cost and low-temperature processing.⁹⁻¹⁴ Over the past years, researchers mostly focused on compositional engineering, interface engineering, additive engineering, and surface passivation approaches in order to boost the device performance as well as stability.¹⁵⁻²⁶ Beside extensive efforts of researchers in this regard, stability is still the main challenge in this field.²⁷⁻³⁰ In fact, finding new effective transporting layers for the PSCs is a good strategy to address this issue.³¹⁻³³ Titanium dioxide (TiO₂) is one of the most commonly used electron transporting layers (ETLs) in the PSCs.³⁴⁻³⁶ However, it suffers from hysteresis and stability issues due to having high amount of oxygen vacancies caused by UV light and also weak charge extraction properties.³⁷ To address this shortening, double-layer ETL and doping strategy have been proposed by many groups, which can improve slightly the efficiency and stability.³⁸⁻⁴⁰ Moreover, employment of new organic and inorganic ETLs such as tin oxide (SnO₂) with better transporting properties could be another solution for this issue.⁴¹ However, these strategies cannot protect the PSCs from the UV illumination. Applying down-shifting materials on the PSCs is an effective way for this purpose.^{42,43} In this study, we propose CdSe/ZnS QDs as a new ETL in the planar PSCs for the first time, with down-shifting property. We fabricate methylammonium lead triiodide (MAPbI₃) perovskite on a thin layer of CdSe/ZnS QDs ETL using evaporation technique. We find that the PSC on CdSe/ZnS QDs ETL with green emission gives us the best efficiency due to more suitable band alignment with respect to the perovskite film than the dots with red emission. We finally achieve a PSC with 18% PCE, indicating a superior UV stability and low hysteresis.

Results and Discussions

Here, we considered CdSe/ZnS QDs (Mesolight) with green (520 nm) and red (640 nm) emissions at ETLs in the PSCs, which have photoluminescence quantum efficiencies (PLQEs) of 85% (Figure S1). Here, we employed CdSe QDs wrapped by ZnS shell due to having higher PLQE and better down-shifting property as compared to the pure QDs layers.⁴⁴ The PLQE has an important role in the efficiency of the device and if it is not high enough, the QDs layer cannot efficiently convert the photons with high energy to the photons with low energy, resulting in lower current density and thus PCE. In this work, we used a solid-state ligand exchange method for deposition of the QDs layer. Then, we employed methylammonium triiodide (MAPbI₃) perovskite with a bandgap of 1.55 eV, as can be found in its UV-visible spectrum (Figure S2). Figure 1a displays schematic of the device structure for the PSCs fabricated on the CdSe/ZnS QDs (green) ETL. As seen in the schematic and its corresponding scanning electron microscopy (SEM), shown in Figure 1b, the device is consisted of ITO/CdSe/ZnS QDs (green)/perovskite/spiro/Au. In this study, we could not use solution processing approach for the deposition of perovskite films, since the perovskite solvent can easily dissolve the underneath QDs layer. Consequently, a layer-by-layer vacuum technique (solvent-free) was employed for the deposition of perovskite film as reported in the literature.^{45,46}

Figure 1c depicts the current density-voltage (J-V) curves of the PSCs fabricated on the TiO₂, CdSe/ZnS QDs with both green and red emissions, which are measured under AM1.5G standard condition. The PV results are summarized in Table 1. The reference device with TiO₂ shows an open circuit voltage (V_{OC}) of 1094 mV, a short circuit current density (J_{SC}) of 22.4 mA/cm², a fill factor (FF) of 74%, and a PCE of 18.15%. In contrast, the PSC on CdSe/ZnS QDs (green) shows lower V_{OC} (1075 mV) and FF (73), but higher J_{SC} (22.9 mA/cm²), resulting in a PCE of 18%, which is comparable with the reference device. We also studied the QDs with both red and green emissions on the device performance. Our PV results indicate that the device on QDs with red emission has lower PCE of 15.8% due to having lower V_{OC} and FF. (V_{OC} : 1023 mV, J_{SC} : 22.9

mA/cm², FF: 68%). However, the QDs-based PSCs (in both cases) shows higher J_{SC}, which can be correlated to the down-shifting property of CdSe/ZnS QDs. Figure 1d demonstrates the external quantum efficiency (EQE) spectra of the corresponding PSCs. Upon integration of the EQE with solar spectrum, the J_{SC} of the devices are estimated as shown in Table 1. The calculated J_{SC} for the PSCs fabricated on TiO₂, QDs (green), and QDs (red) are 21.7 mA/cm², 22.3 mA/cm², 22.1 mA/cm², respectively, which are greatly consistent with the J-V measurement. As seen in Figure 1d, the EQE of the QDs-based devices is higher in the UV region as compared to the TiO₂ device. This is originated from down-shifting property of the CdSe/ZnS QDs, where the photons with high energy (from UV region) are converted to the photons with lower energy (at 520 nm or 640 nm), which results in higher EQE in the UV region.⁴³ Notably, the TiO₂ ETL absorbs the UV light and thus increases the parasitic absorption (lower EQE).

Figure S3 shows the statistic of PV parameters for the corresponding PSCs. The results indicate that the average values of the PV parameters are in good agreement with the best performing PSCs (Table 1). In fact, the average value of PCE for the QDs (green) is 17.6%, which is comparable with the TiO₂ PSCs (17.85%). The devices on QDs (red) shows an average PCE of 15.3%, mainly due to the lower values of V_{OC} and FF. We also monitored the average value of hysteresis index (HI% = ((PCE_{reverse} - PCE_{forward})/PCE_{reverse}) × 100) of these devices, as can be found in Figure S4. As seen, the average value of HIs for the QDs-based PSCs are 2.5% (green) and 2.6% (red), much lower than that of TiO₂ devices (4.05%). This result can be ascribed to better charge transfer property of QDs ETL compared with TiO₂.

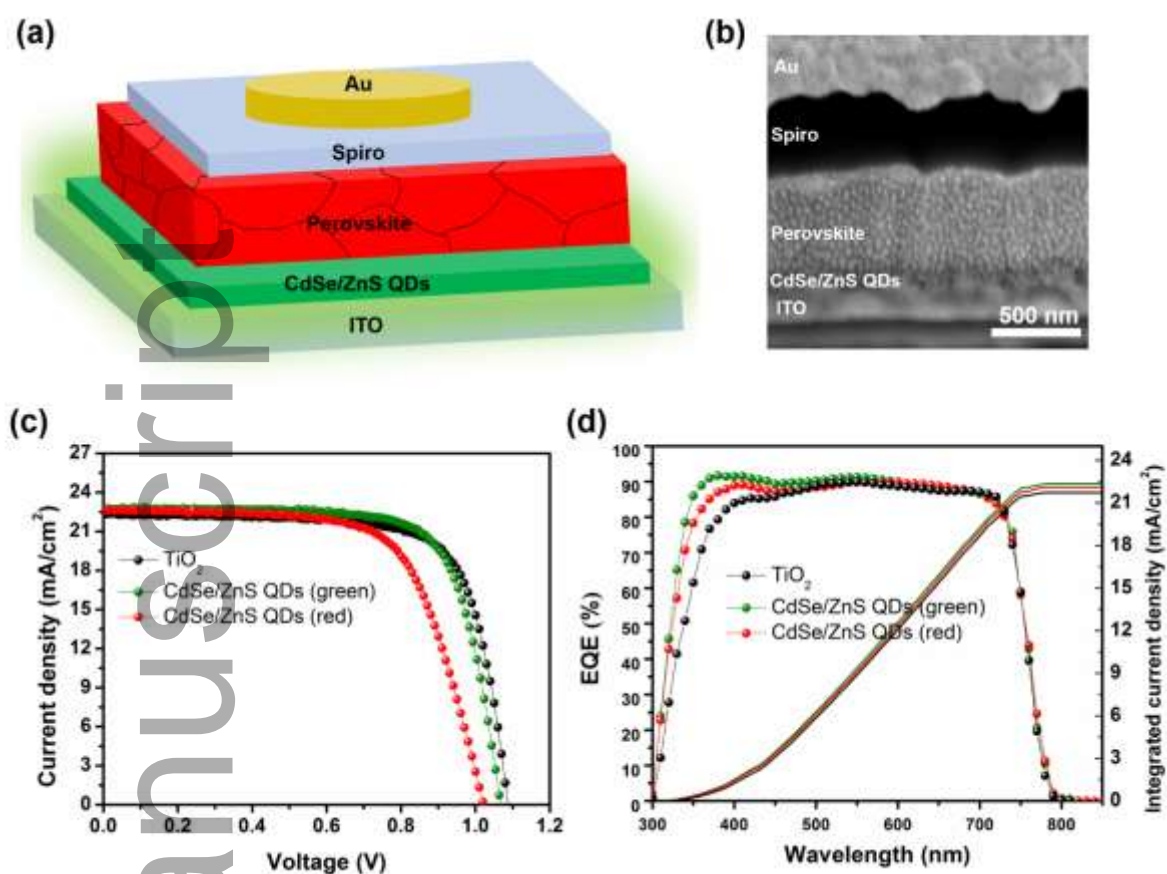


Figure 1. (a) Schematic and (b) cross-sectional SEM image of the PSCs fabricated on CdSe/ZnS QDs ETL with green emission. (c) J-V curves and (d) EQE spectra of the PSCs with TiO₂ and CdSe/ZnS QDs ETLs.

Table 1. PV parameters of the PSCs fabricated on TiO₂ and CdSe/ZnS QDs ETLs measured under reverse scan

Device	V _{oc} (mV)	J _{sc} (mA/cm ²)	FF (%)	PCE (%)	J _{sc} from EQE (mA/cm ²)
TiO ₂	1094	22.4	74	18.15	21.7
CdSe/ZnS QDs (green)	1075	22.9	73	18	22.3
CdSe/ZnS QDs (red)	1023	22.7	68	15.8	22.1

We also optimized the thickness of CdSe/ZnS QDs ETLs by measuring the efficiency of the PSCs fabricated on the QDs with different thicknesses. Figure S5 depicts the variation of PCE versus the QDs (green) thickness. The result indicates that 20 nm is the optimum thickness of the QDs layer. In fact, by increase the thickness over this value, the transmittance is dropped, resulting in lower J_{SC} , and thus reduced efficiency. Consequently, there is a trade-off between transmittance and down-shifting property for these devices.

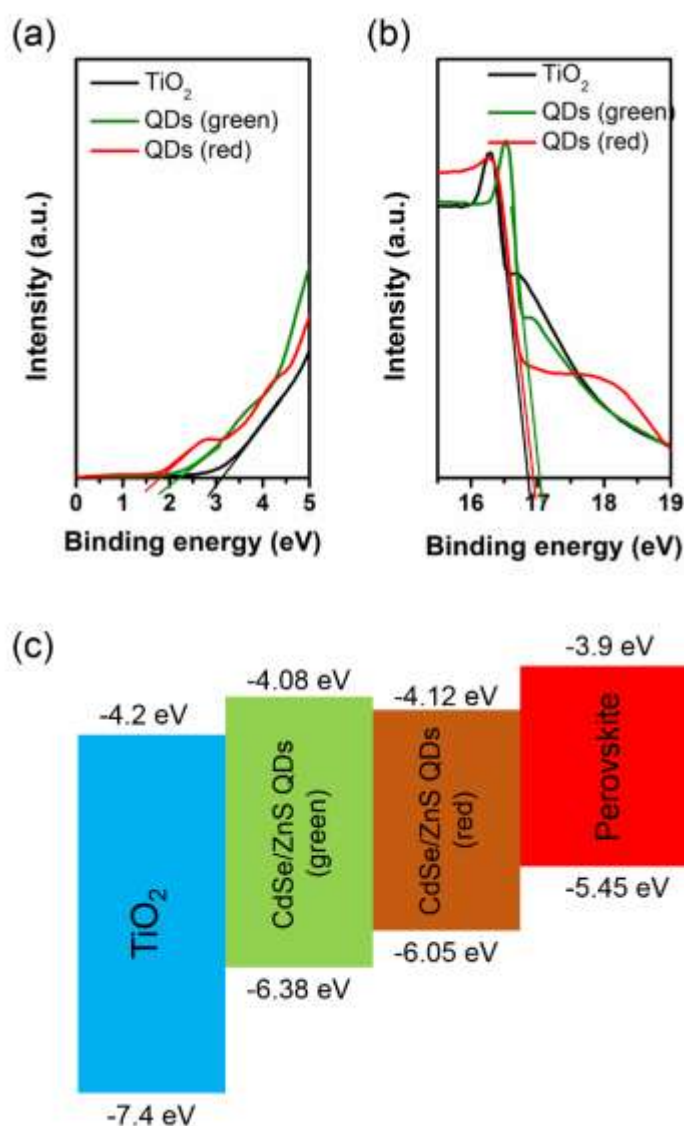


Figure 2. (a,b) UPS measurement of the TiO₂, CdSe/ZnS QDs (green), and CdSe/ZnS QDs (red) ETLs. (c) Band diagram of the PSCs fabricated on the corresponding ETLs.

In order to interpret the PV results obtained from the PSCs fabricated on TiO₂ and QDs ETLs, ultraviolet photoelectron spectroscopy (UPS) is employed to analyze the band alignment in the corresponding devices. Figure 2a,b displays the UPS measurement for the TiO₂ and QDs (red and green) ETLs. Based on the UPS results, the valence bands (VBs) of the TiO₂, QDs (green), and QDs (red) are estimated to be -7.4 eV, -6.38 eV, and -6.05 eV, respectively. Using their optical bandgaps and VBs, we calculate the conduction bands (CBs) of the TiO₂, QDs (green), and QDs (red) to be -4.2 eV, -4.08 eV, and -4.12 eV, respectively. Based on these data and the literature⁴⁴, we plotted the band diagram of the corresponding PSCs, as shown in Figure 2c. As seen, the band offset between the CBs of QDs (green) and perovskite is only 180 meV, which is much lower than those of the TiO₂ and QDs (red) ETLs. This can facilitate the charge transfer between the perovskite film and QDs (green) ETL, resulting in a lower recombination and improved J_{SC}. In another hand, the bandgap of the TiO₂ ETL is higher than QDs-based ETLs. As a result, TiO₂ ETL can more efficiently stop the hole transfer from perovskite film to the ITO electrode as compared its counterparts and thus the TiO₂-based PSCs show higher V_{OC}. Since the QDs (green) has also larger bandgap than the QDs (red), there is less chance for the holes in the VB of the perovskite to recombine with the electrons in the ITO glass. Moreover, the charge transfer in QDs (green) devices is smoother due to less band offset at the ETL/perovskite interface as compared to the QDs (red). Consequently, the QDs (green) is a better choice for the PSCs in terms of lower recombination and higher PV parameters.^{47,48}

Figure 3a and 3b depict the top-view SEM images of the perovskite films deposited on TiO₂ and QDs (green) ETLs, respectively. As seen, both films show the same morphology with almost similar grain size. We also measured the transmittance spectra of both TiO₂ and QDs (green) ETLs, as can be found in Figure 3c. As seen, both films have over 80% transmittance above 400 nm wavelength. In fact, the QDs film has lower transmittance, particularly below 430 nm due to its absorption. The steady state photoluminescence (PL) spectroscopy indicates a strong PL quenching

for the perovskite film deposited on QDs (green) as compared to its counterpart, which can be correlated to its better charge transfer (Figure 3d).

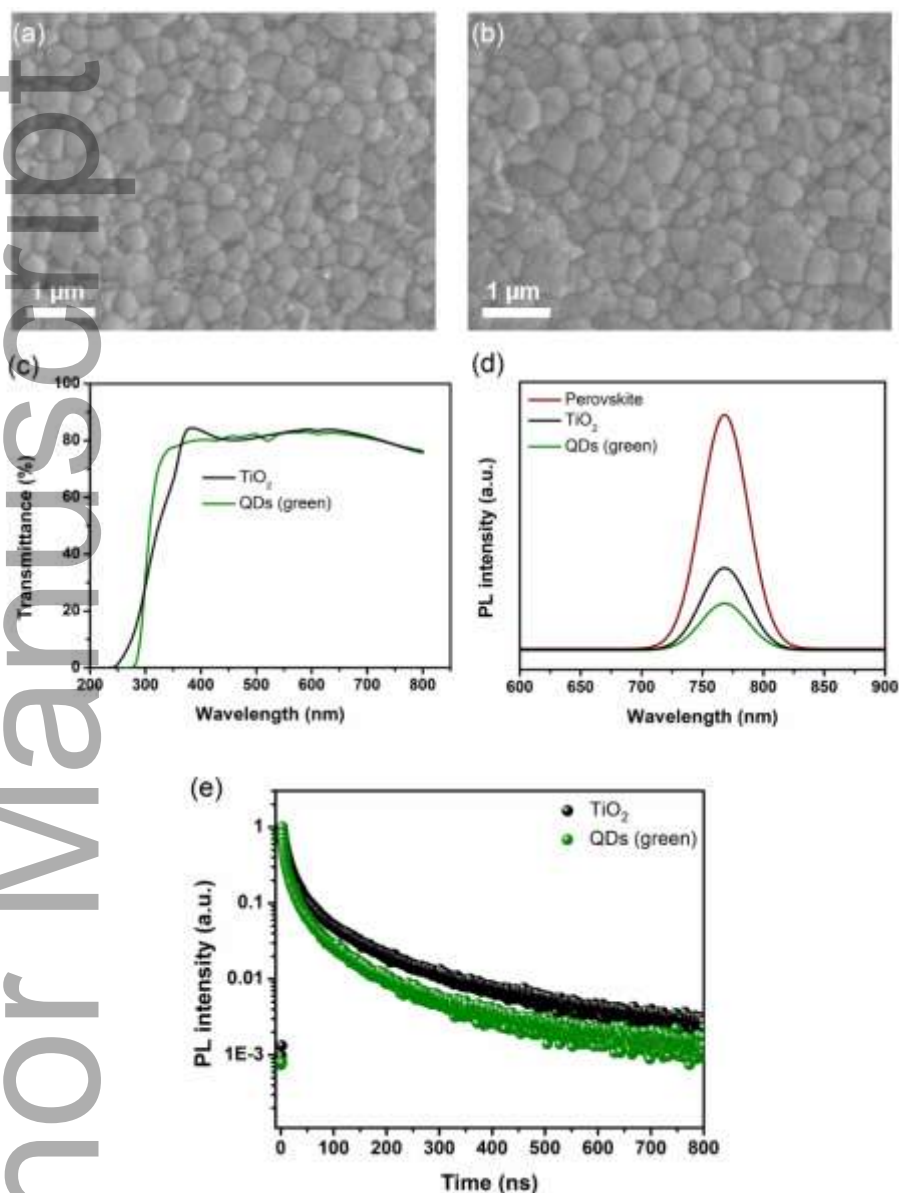


Figure 3. Top-view SEM images of perovskite films on (a) TiO₂ and (b) CdSe/ZnS QDs (green) ETLs. (c) Transmittance spectra of the corresponding ETLs. (d) Photoluminescence spectra and (e) time-resolved photoluminescence of the perovskite deposited on TiO₂ and CdSe/ZnS QDs (green) ETLs.

Additionally, we measured time-resolved PL spectra of perovskite films on both TiO₂ and QDs (green) ETLs, as shown in Figure 3e. Table S1 summarizes the fitting parameters of the

corresponding TRPL curves. This result confirms the stronger quenching effect for the QDs (green) sample as compared to the TiO_2 one, due to having shorter PL lifetime.

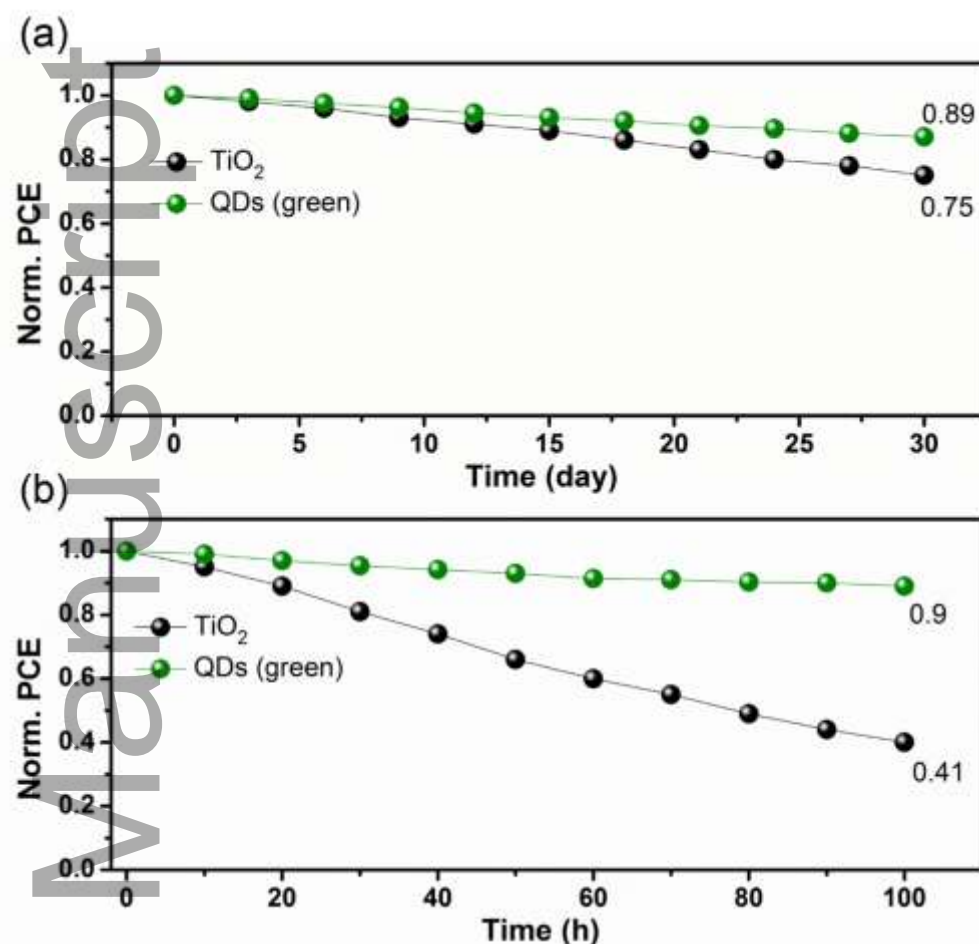


Figure 4. (a) Shelf-life stability and (b) UV stability of the PSCs fabricated on TiO_2 and CdSe/ZnS QDs (green) ETLs.

Stability under light and in ambient condition is still the main challenge for commercialization of the PSCs.² In this study, the main purpose of using CdSe/ZnS QDs as an ETL is improving the stability of the device. Since this ETL has down-shifting property, it can convert photons with high energy to the ones with lower energy and thus protect the device from degradation. Figure 4a shows the shelf-life stability test of the PSCs with different ETLs kept in ambient condition (45% relative humidity (RH) under dark condition and at room temperature). As seen, the device with QDs (green) ETL retains 89% of its original PCE after 30 days, which is better than the TiO_2 -based device (75%). Additionally, the UV stability of the corresponding PSCs are also measured for 100

h, as shown in Figure 4b. Interestingly, the PSCs with the QDs (green) ETL maintains 90% of its initial PCE over 100 h, which highlights the potential of QDs ETL for improving the operational stability. In contrast, the device with TiO₂ ETL has 59% PCE loss, indicating its poor stability under UV light. Besides, we also evaluated the thermal stability of the corresponding PSCs at 60° C, as shown in Figure S6. Our results indicate that the device on QDs layer has slightly better thermal stability, which can be corresponded to the better interface of QDs layer/perovskite.

Conclusions

In conclusion, we propose a new ETL, CdSe/ZnS QDs for the fabrication of UV-stable PSCs. We deposited a thin layer of the QDs as an ETL using solid-state ligand exchange method. We employed the QDs with both red and green emissions and compared them with the commonly used TiO₂ ETL. Our characterization results indicate that the QDs (green) layer has a suitable band alignment and charge transfer property better than the TiO₂ ETL with respect to the MAPbI₃ perovskite film. From the PV results, a PSC with PCE of 18% is achieved using the QDs (green), which is comparable with device based on TiO₂ ETL. Finally, we discover that the QDs (green) ETL drastically improves the UV-stability of the PSCs, which is a great advantage for the commercialization of this type of solar cell.

Conflict of Interests

There is no conflict to declare.

Acknowledgement

This work was supported by Iran Nanotechnology Innovation Council. M.M.T would like to acknowledge the research laboratory of electronics (RLE) at Massachusetts Institute of Technology.

Experimental section

Device fabrication:

The prepatterned Indium-coated tin oxide (ITO, TFD) glasses were cleaned by sonification of in baths of detergent, Deionized water, acetone and isopropanol, respectively, for 20 min. Then the substrates were further cleaned by oxygen plasma for 10 min. The TiO₂ compact layer was deposited at 4000 rpm for 30 s from a solution of titanium diisopropoxide bis(acetylacetonate) (75% in 2-propanol, Sigma-Aldrich) with a concentration of 0.15 mM, followed by annealing at 450 °C for 30 min. In case of CdSe/ZnS QDs (Mesolight) with core-shell structure, a solution of 1-Dodecanethiol-capped QDs (50 mg/mL in octane) was prepared and deposited at 2500 rpm for 30 s. The CdSe core size is 8-10 nm and the ZnS shell size is 2-3 nm. A solid-state ligand exchange technique⁴⁹⁻⁵² was used to replace 1-Dodecanethiol with 3-mercaptopropionic acid (MPA, 1% vol in methanol). We deposited the QDs layer twice to obtain optimized thickness. In each step, we washed away the unbonded ligands using methanol three times and performed spin drying. After preparing the ETL, perovskite film was deposited using layer-by-layer vacuum approach, as can be found in the literature. We deposited MAPbI₃ perovskite film from PbI₂ and methylammonium iodide powders located in two separated boats. After finishing the evaporation, the perovskite film was formed by annealing at 90 °C for 10 min. For hole transporting layer (HTL), a solution of Spiro-OMeTAD (80 mg mL⁻¹ in chlorobenzene) mixed with 17.5 μL of Li-bis(trifluoromethanesulfonyl)imide (Li-TFSI) in acetonitrile (500 mg mL⁻¹) and 28.5 μL of 4-*tert*-butylpyridine (*t*BP) was prepared and spin-coated at 4000 rpm for 20 s. Finally, gold electrode with 100 nm thickness was thermally evaporated on the substrates as a back contact through a shadow mask.

Film characterization

Scanning electron microscopy (SEM, ZEISS Merlin) was employed to evaluate the morphology of the perovskite films and the device cross-section. For optical study, photoluminescence (Horiba Jobin Yvon Ltd, excitation wavelength=460 nm) and UV-visible (Varian Cary 5) were used. For TRPL measurement, a diode laser with pulse width of 49 picosecond was used and the excitation wavelength was fixed to $\lambda=405$ nm. For fitting purpose, an exponential equation ($I(t) = a_i \exp(-t/\tau_i)$)

was employed (a_i is the amplitude and τ_i is the lifetime). UPS measurement was recorded using AXIS NOVA (Kratos Analytical Ltd, UK) by employing a He I (21.2 eV) photon source.

Device measurement

To measure the solar cells, Keithley (model 2400, USA) and a xenon lamp (Oriel, USA, 450 W) were employed. All devices were measured under AM1.5G standard condition by using a shadow mask. During the measurement, the scan rate and the dwell time were 10 mV/s and 15 s, respectively. For EQE measurement, a commercial apparatus (Arkeo-Ariadne, Cicci Research s.r.l.) was used equipped with xenon lamp (300 W). For UV stability test, the devices were exposed to the UV light in a nitrogen-filled glovebox. The light intensity was 100 mW/cm² in this measurement.

References

1. X. Zheng, B. Chen, J. Dai, Y. Fang, Y. Bai, Y. Lin, H. Wei, X. C. Zeng, J. Huang, *Nat. Energy*, **2017**, 2, 17102.
2. M. M. Tavakoli, W. Tress, J. V. Milić, D. Kubicki, L. Emsley, M. Grätzel, *Energy Environ. Sci.* **2018**, 11, 3310.
3. M. M. Tavakoli, A. Waleed, L. Gu, D. Zhang, R. Tavakoli, B. Lei, W. Su, F. Fang, Z. Fan, *Nanoscale*, **2017**, 9, 5828-5834.
4. M. Stolterfoht, C. M. Wolff, J. A. Márquez, S. Zhang, C. J. Hages, D. Rothhardt, S. Albrecht, P. L. Burn, P. Meredith, T. Unold, D. Neher, *Nat. Energy*, **2018**, 3, 847.
5. M. M. Tavakoli, S. M. Zakeeruddin, M. Grätzel, Z. Fan, *Adv. Mater.* **2018**, 30, 1705998.
6. P. Yadav, S. H. Turren-Cruz, D. Prochowicz, M. M. Tavakoli, K. Pandey, S. M. Zakeeruddin, M. Grätzel, A. Hagfeldt, M. Saliba, *J. Phys. Chem. C*, **2018**, 122, 15149-15154.
7. K. Choi, J. Lee, H. I. Kim, C. W. Park, G. W. Kim, H. Choi, S. Park, S. A. Park, T. Park, *Energy Environ. Sci.* **2018**, 11, 3238-3247.
8. M. Yavari, M. Mazloum-Ardakani, S. Gholipour, M. M. Tavakoli, S. H. Turren-Cruz, N. Taghavinia, M. Grätzel, A. Hagfeldt, M. Saliba, *Adv. Energy Mater.* **2018**, 8, 1800177.
9. J. Cao, B. Wu, R. Chen, Y. Wu, Y. Hui, B. W. Mao, N. Zheng, *Adv. Mater.* **2018**, 30, 1705596.
10. M. M. Tavakoli, L. Gu, Y. Gao, C. Reckmeier, J. He, A. L. Rogach, Y. Yao, Z. Fan, *Sci. Rep.* **2015**, 5, 14083.

11. National Center for Photovoltaics (NCPV) at the National Renewable Energy Laboratory (NREL); www.nrel.gov/pv/assets/images/efficiency-chart.png.
12. M. M. Tavakoli, D. Bi, L. Pan, A. Hagfeldt, S.M. Zakeeruddin, M. Grätzel, *Adv. Energy Mater.* **2018**, 8, 1800275.
13. N. J. Jeon, J. H. Noh, W. S. Yang, Y. C. Kim, S. Ryu, J. Seo, S. I. Seok, *Nature*, **2015**, 517, 476.
14. Q. Zhang, M. M. Tavakoli, L. Gu, D. Zhang, L. Tang, Y. Gao, J. Guo, Y. Lin, S. F. Leung, S. Poddar, Y. Fu, *Nat. Commun.* **2019**, 10, 727.
15. M. M. Tavakoli, R. Tavakoli, P. Yadav, J. Kong, *J. Mater. Chem. A* **2019**, 7, 679-686.
16. M. Kim, G. H. Kim, T. K. Lee, I. W. Choi, H. W. Choi, Y. Jo, Y. J. Yoon, J. W. Kim, J. Lee, D. Huh, H. Lee, *Joule*, 2019, 3, .2179-2192.
17. D. Prochowicz, R. Runjhun, M. M. Tavakoli, P. Yadav, M. Saski, A. Q. Alanazi, D. J. Kubicki, Z. Kaszkur, S. M. Zakeeruddin, J. Lewiński, M. Grätzel, *Chem. Mater.* **2019**, 31, 1620-1627.
18. D. Luo, W. Yang, Z. Wang, A. Sadhanala, Q. Hu, R. Su, R. Shivanna, G. F. Trindade, J. F. Watts, Z. Xu, T. Liu, K. Chen, F. Ye, P. Wu, L. Zhao, J. Wu, Y. Tu, Y. Zhang, X. Yang, W. Zhang, R. H. Friend, Q. Gong, H. J. Snaith, R. Zhu, *Science*, **2018**, 360, 1442-1446.
19. T. Li, Y. Pan, Z. Wang, Y. Xia, Y. Chen, W. Huang, *J. Mater. Chem. A*, **2017**, 5, 12602-12652.
20. P. Cui, D. Wei, J. Ji, H. Huang, E. Jia, S. Dou, T. Wang, W. Wang, M. Li, *Nat. Energy*, 2019, 4, 150-159.
21. Q. Ma, S. Huang, X. Wen, M. A. Green, A. W. Ho-Baillie, *Adv. Energy Mater.* **2016**, 6, 1502202.
22. M. H. Gharahcheshmeh, M. M. Tavakoli, E. F. Gleason, M. T. Robinson, J. Kong, K. K. Gleason, *Sci. Adv.* **2019**, 5, eaay0414.
23. X. Zheng, B. Chen, J. Dai, Y. Fang, Y. Bai, Y. Lin, H. Wei, X. C. Zeng, J. Huang, *Nat. Energy*, 2017, 2, 1-9.
24. W. Ke, D. Zhao, C. R. Grice, A. J. Cimaroli, G. Fang, Y. Yan, *J. Mater. Chem. A*, **2015**, 3, 23888-23894.
25. M. M. Tavakoli, R. Tavakoli, Z. Nourbakhsh, A. Waleed, U. S. Virk, Z. Fan, *Adv. Mater. Interfaces* **2016**, 3, 1500790.
26. X. Zheng, Y. Hou, C. Bao, J. Yin, F. Yuan, Z. Huang, K. Song, J. Liu, J. Troughton, N. Gasparini, C. Zhou, *Nat. Energy*, 2020, 5, 131-140.
27. J. Zhao, R. Tavakoli, M. M. Tavakoli, *Chem. Commun.* 2019, 55, 9196-9199.

28. M. M. Tavakoli, H. T. Dastjerdi, D. Prochowicz, P. Yadav, R. Tavakoli, M. Saliba, Z. Fan, J. *Mater. Chem. A*, **2019**, *7*, 14753-14760.
29. N. G. Park, M. Grätzel, T. Miyasaka, K. Zhu, K. Emery, *Nat. Energy*, **2016**, *1*, 16152.
30. M. M. Tavakoli, J. Zhao, R. Po, G. Bianchi, A. Cominetti, C. Carbonera, J. Kong, *Adv. Funct. Mater.* **2019**, *29*, 1905887.
31. J. W. Lee, H. S. Kim, N. G. Park, *Acc. Chem. Res.*, **2016**, *49*, 311-319.
32. M. M. Tavakoli, D. Prochowicz, P. Yadav, R. Tavakoli and M. Saliba, *Eng. Sci.*, **2018**, *3*, 48-
33. M. M. Tavakoli, H. T. Dastjerdi, J. Zhao, K. E. Shulenberger, C. Carbonera, R. Po, A. Cominetti, G. Bianchi, N. D. Klein, M. G. Bawendi, S. Gradecak, J. Kong, *Small*, **2019**, *15*, 1900508.
34. A. Waleed, Q. Zhang, M. M. Tavakoli, S. F. Leung, L. Gu, J. He, X. Mo, Z. Fan, *Sci. Bull.* **2016**, *61*, 86-91.
35. D. Prochowicz, M. M. Tavakoli, A. Solanki, T. W. Goh, K. Pandey, T. C. Sum, M. Saliba and P. Yadav, *J. Mater. Chem. A*, **2018**, *6*, 14307–14314.
36. N. J. Jeon, J. H. Noh, W. S. Yang, Y. C. Kim, S. Ryu, J. Seo, S. I. Seok, *Nature*, **2015**, *517*, 476-480.
37. Z. Yang, B. H. Babu, S. Wu, T. Liu, S. Fang, Z. Xiong, L. Han, W. Chen, *Solar Rrl*, 2020, *4*, 1900257.
38. M. M. Tavakoli, F. Giordano, S. M. Zakeeruddin, M. Grätzel, *Nano Lett.* **2018**, *18*, 2428–2434.
39. R. Wang, M. Mujahid, Y. Duan, Z. K. Wang, J. Xue, Y. Yang, *Adv. Funct. Mater.* **2019**, *29*, 1808843.
40. J. Song, W. Zhang, D. Wang, K. Deng, J. Wu, Z. Lan, *Solar Energy*, **2019**, *185*, 508-515.
41. M. M. Tavakoli, P. Yadav, D. Prochowicz, M. Sponseller, A. Osherov, V. Bulović, J. Kong, *Adv. Energy Mater.* **2019**, *9*, 1803587.
42. F. Bella, G. Griffini, J. P. Correa-Baena, G. Saracco, M. Grätzel, A. Hagfeldt, S. Turri, C. Gerbaldi, *Science* **2016**, *354*, 203-206.
43. H. T. Dastjerdi, D. Prochowic, P. Yadav, M. M. Tavakoli, *Sustain. Energy Fuels*, **2019**, *3*, 3128-3134.
44. J. Hao, H. Liu, J. Miao, R. Lu, Z. Zhou, B. Zhao, B. Xie, J. Cheng, K. Wang, M. H. Delville, *Sci. Rep.* **2019**, *9*, 1-8.

45. M. M. Tavakoli, A. Simchi, X. Mo, Z. Fan, *Mater. Chem. Front.* **2017**, *1*, 1520-1525.
46. M. M. Tavakoli, P. Yadav, D. Prochowicz, R. Tavakoli, M. Saliba, *J. Phys. D Appl. Phys.* **2018**, *52*, 034005.
47. T. Minemoto, M. Murata, *Sol. Energy Mater. Sol. Cells*, **2015**, *133*, 8-14.
48. W. Zhu, Z. Zhang, W. Chai, Q. Zhang, D. Chen, Z. Lin, J. Chang, J. Zhang, C. Zhang, Y. Hao, *ChemSusChem*, 2019, *12*, 2318-2325.
49. A. Tayyebi, M. M. Tavakoli, M. Outokesh, A. Shafiekhani, A. Simchi, *Ind. Eng. Chem. Res.* **2015**, *54*, 7382-7392.
50. M. M. Tavakoli, A. Simchi, Z. Fan, H. Aashuri, *Chem. Commun.* **2016**, *52*, 323-326.
51. M. M. Tavakoli, A. Simchi, H. Aashuri, *Mater. Chem. Phys.* **2015**, *156*, 163-169.
52. H. Tavakoli Dastjerdi, R. Tavakoli, P. Yadav, D. Prochowicz, M. Saliba, M. M. Tavakoli, *ACS Appl. Mater. Interfaces*, **2019**, *11*, 26047-26052.

TOC

CdSe/ZnS quantum dots with core-shell structure is a great electron transfer layer for the fabrication of high efficiency perovskite solar cells up to 18% and improving the UV-stability of the device.

